Conductive layers in diamond formed by hydrogen ion implantation and annealing

ARTICLE *in* NUCLEAR INSTRUMENTS AND METHODS IN PHYSICS RESEARCH SECTION B BEAM INTERACTIONS WITH MATERIALS AND ATOMS · JULY 2012

Impact Factor: 1.12 · DOI: 10.1016/j.nimb.2011.08.050

Nuclear Instruments and Methods in Physics Research B 282 (2012) 100–107

Contents lists available at SciVerse ScienceDirect

Nuclear Instruments and Methods in Physics Research B

journal homepage: www.elsevier.com/locate/nimb

Conductive layers in diamond formed by hydrogen ion implantation and annealing

V.P. Popov [a,*], L.N. Safronov [a], O.V. Naumova [a], D.V. Nikolaev [a], I.N. Kupriyanov [b], Yu.N. Palyanov [b]

[a] A.V. Rhzanov Institute of Semiconductor Physics, SB RAS, 630090 Novosibirsk, Russia
[b] V.S. Sobolev Institute of Geology and Mineralogy, SB RAS, 630090 Novosibirsk, Russia

ARTICLE INFO

Article history:
Available online 16 September 2011

Keywords:
Diamond
Hydrogen implantation
HPHT annealing
VRH conductivity

ABSTRACT

High conductivity is extremely difficult to obtain in diamond due to its wide band gap and low solubility of dopands. The goal of the investigation was to form a conductor inside HPHT synthetic diamond plates with initial high sheet resistivity ρ_s ($\sim 10^{12}$ Ω/sq) for 400 μm thickness. We used metastable character of diamond structures relative to the graphitization of defective layers formed by 50 keV hydrogen molecular ions at high fluence $\Phi = (1-13) \times 10^{16}$ cm^{-2} ion implantation. High temperature (HT) (500–1600 °C) and vacuum or high pressure (VP/HP) (3×10^{-3}/4×10^{9} Pa) thermal annealing were chosen to provide the annealing regimes where the graphitic carbon is the most stable phase. Sheet resistance, dropped down up to nine orders of magnitude ($\rho_s \sim 10^3$ Ω/sq), as well as Raman spectroscopy, and AFM measurements were used to determine electrical, optical and geometrical properties of multilayered heterostructures formed in the set of experiments. Temperature dependences of the conductivity show, that after highest fluencies and annealing temperatures the conductivity is quasimetallic and electronic system is above metal–insulator transition (MIT). At lower fluences and/or annealing temperatures the system is under MIT with the transport of charge carriers being well described by variable range hopping (VRH) mechanism with variable decay length of wave function for localized states. Two or three order of magnitude differences in the conductivity in VP and HP annealed samples are attributed with the higher dimensions of graphite nanocrystals in the case of vacuum annealing. This suggestion coincides with Raman spectra and optimum hopping length for carrier jumps in VRH model for conductivity in the buried layers.

1. Introduction

Production of electronic devices is not possible without a wide low-impedance semiconductor layer and metallic contacts. Problem for diamond low-resistivity contacts is particularly acute because of the high resistance even at huge levels of impurity concentration doping (>1×10^{18} cm^{-3}). The high level of ionization potentials (0.37 and 0.62 eV for shallow acceptor boron and donor phosphorus atoms, respectively) and low diffusivity of impurities make it impossible to establish contact areas by thermal indiffusion [1,2]. Another problem is the pinning of the Fermi level due to surface conditions. Moreover for boron-doped diamond, contact properties are highly dependent on the surface states. Hydrophobic surfaces filled by hydrogen have a high conductivity and low value of contact barriers with metals while hydrophilic oxidized surface has low conductivity and large Schottky barriers.

Ion implantation of doped impurities like boron or phosphorus at fluences above a certain critical value (Φ_c) causes amorphisation followed by graphitization of implanted layers during thermal treatments [2–4]. Light ions produce fewer defects in nuclear collisions, so the critical fluence to them is substantially higher, and concentrations of implanted atoms close to the concentrations of introduced defects. More than a dozen articles are devoted to study and applications of graphitization due to implantation by light ions (H^+, D^+, He^+) [5–13,20–22], but the mechanisms of electrical conductivity in the exposed layers depending on the phase composition and doping have not been extensively investigated. In particular, Gippius et al. studied visible light transmittance changes in diamond after irradiation with H^+ and He^+ ions and after annealing as well as changing the resistance of the buried layer in dependence on the fluence [4–6].

Electrical contacts to buried layers were produced by multienergy ion implantation at fluences above the critical one Φ_c for contact area graphitization during subsequent thermal treatments. In order to achieve the graphitization in the buried layer irradiated with hydrogen ions, implantation fluence should exceed 6×10^{16} cm^{-2}, while they specifically noted that the introduction of critical dose for H^+ ions is missing, because graphitization has also been seen at lower doses, but for higher temperatures of annealing. The concentration of hydrogen ions that caused graphitization was approximately higher than 1 at.% at the peak of im-

* Corresponding author. Tel.: +7 383 333 2493.
E-mail addresses: popov@isp.nsc.ru, popovorama@gmail.com (V.P. Popov).

0168-583X/$ - see front matter © 2011 Elsevier B.V. All rights reserved.
doi:10.1016/j.nimb.2011.08.050

planted profile. The gapless graphite layer was not observed at all fluences which prevented the authors from completing electrical measurements [7]. Increased fluences resulted only in increasing of various sizes of blisters and flakes on the diamond surface [8]. Total concentration of vacancies created during implantation did not exceed 5×10^{21} cm^{-3} and the intensity of the EPR-active centers decreased by two order of magnitude after annealing at 1200 °C [9]. Unlike hydrogen ions continuous conductive layers were formed above a certain critical fluence Φ_c of D^+ and He^+ after annealing, and similar to polycrystalline graphite structural, electrical and optical properties were observed, namely close to a linear negative temperature coefficient of resistance $-1.5 \times 10^{-4}\ \Omega\ K^{-1}$ in the temperature range 50–400 K [10].

Recently, similar results were obtained by Olivero et al. They used focused microbeams of H^+, He^+ and C^+ ions with MeV energies for forming conductive tracks and waveguides for visible light inside diamond [11–13]. For contact to layers metallic masks with variable thickness were used in the form of half-spherical Au balls with diameter up to 50 μm [11–13]. Conflicting results were obtained. Thus, the investigated temperature dependence of conductivity was described in the article [12] by the model [14,15] of hopping conductance with variable length jump and density of states near Fermi level $N_{EF} = 5.5 \times 10^{17}$ cm^{-3} eV^{-1}, while the same authors described a migration of charge carriers by the Baskin's model of transport through the subband of vacancies [16]. The difference in the results [11,12] was attributed to the lack of good electrical contact to the buried layers according to TEM cross-sectional investigation [13].

Formation of heterostructures with sacrificial graphite-like buried layer were investigated in diamond after implantation of light and self ions and thermal annealing [17–21]. This layer was used to create diamond shaping in the processes leaving by galvanic and chemical etching lift-off diamond film, cavities, membranes and nanowire for photonic crystals [17], magnetic and spin devices for quantum information processes [18] and nanoelectro-mechanical-systems (NEMS) [19]. The main disadvantage of the method for creating lift-off layer is residual defects, especially noticeable when the diamond layer thickness is near ~100 nm. To reduce the defects in the lift-off layer, M. Liao et al. used epitaxial overgrowth of diamond layer by MW-plasma PCVD method on the previously implanted diamond by C^+ ions with keV energy [19]. Residual defects in lift-off layer were observed after implantation of light He^+ ions by XTEM [20,21]. These defects have a pronounced impact on the electrical and optical properties of layers and limit their potential applications in optoelectronics and spintronics [22].

The goal of this work was exploring the possibility of using lightweight H^+ ions with tens of keV energy to create hidden conductive layers in bulk of insulating diamond with thicknesses up to $100 \div 200$ nm and low defect concentration in the upper few tens nanometer thick layer, which could be useful in the formation of optoelectronic and spintronic devices for future quantum computing.

2. Experimental

Synthetic high pressure high temperature (HPHT) diamond single-crystals of the type Ib, IIb and IIa with substitutional nitrogen, or boron impurity atoms, or pure diamond with impurity level below 1 ppm, respectively, were grown in V.S. Sobolev Institute of Geology and Mineralogy, Novosibirsk [23]. The crystals were sliced on the 300–500 μm plates with the area up to 40 mm^2 by cleavage along {1 1 1} planes. As cleaved DC-series and polished NG-series with 100–200 ppm of nitrogen (type Ib), B-series with 1–10 ppm of boron (type IIb) and NF-series without impurities (<1 ppm, type IIa) of samples were used for the experiments.

These plates were irradiated by different fluences of 1×10^{16}–1.3×10^{17} cm^{-2} by 50 keV hydrogen molecular ions H_2^+. As cleaved and polished plates were used for 120 keV N^+ ion implantation through 10 μm Al foil placed on the plates or through photolithographically deposited 1 μm Al masks on the polished surfaces to form electrical contact pads. These pads are shown on the Fig. 1. Tungsten needles were used for electrical contacts to the pads during *I–V* measurements using NI Lab View™ set up and software.

The H^+ and N^+ ion irradiated samples were annealed in a protective CO atmosphere in graphite crucible at temperatures 500–1000 °C (LPHT), or in a high vacuum (10^{-3} Pa) chamber at temperatures 1000–1600 °C (VPHT), or under high pressure (4 GPa) and high temperature 1200 °C (HPHT). The latter thermal treatment (HPHT) was provided by the same units that were used for HPHT growth of diamond crystals [23]. The results of the ion induced surface swelling (AFM), electrical (Van-der-Pauw) and optical (Raman spectra) measurements are presented in the next part of the article. To avoid surface conductivity all samples were chemically etched before electrical measurements in boiled diluted acid solution and then rinsed in isopropyl spirits and deionized water. Structural and phase changes were studied with a confocal micro-Raman Horiba J.Y.™ T6400 spectrometer with single mode Ar-ion laser at $\lambda = 514.5$ nm and with NT-MDT™ AFM scanners in tape and phase modes.

3. Results

3.1. Ion induced surface swelling and resistance measurements

To provide good electrical contacts to a buried hydrogen implanted layer, a preliminary study was performed for the conductivity of the layers formed in diamond by implantation of

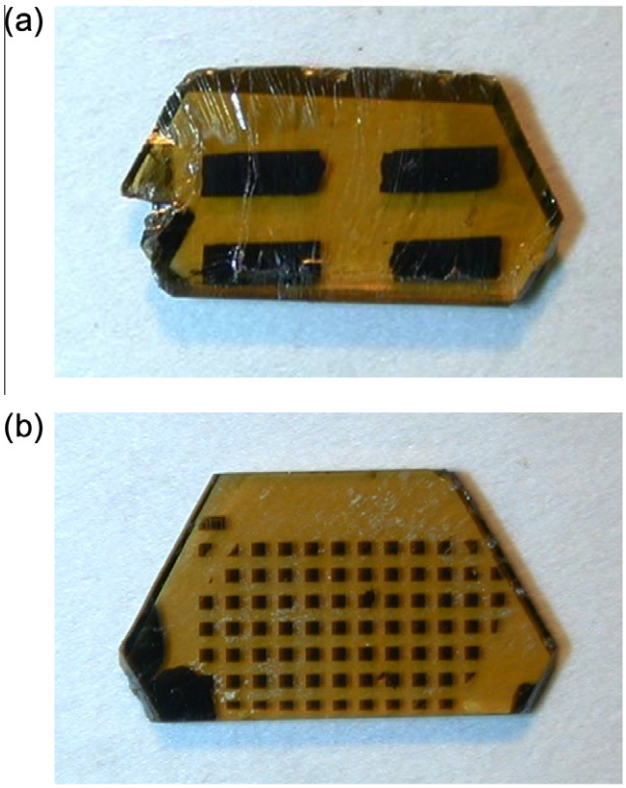

Fig. 1. (a) Map of 0.5×2 mm^2 contact pads on cleaved surface of diamond plate (DC-series) formed by N^+ ion implantation through 10 μm Al foil placed above; (b) the same but for 200×200 μm^2 pads photolithographically formed 1 μm Al mask on polished diamond surface (NG-series).

different doses of nitrogen ions. We investigated the dependences of the step height formed due to the swelling of the N^+ implanted areas and the resistivity inside the pads on the annealing temperature (Fig. 2). It is seen from Fig. 2, that the dose of nitrogen ions higher than 3×10^{16} cm^{-2} is quite enough to obtain low-resistivity (<1 kΩ/sq) contact pads even for temperatures lower than 1000 °C. The nitrogen dose 3.5×10^{16} cm^{-2} was used for all further experiments to make contact pads for buried layers and current–voltage (I–V) characteristic measurements.

Fig. 3 shows, that the conductivity between two neighbor pads (on inset) has pure ohmic character for NG samples annealed at 900 and 1000 °C during 1 h for highest and lowest fluences of hydrogen molecular ions H_2^+, respectively. The difference in conductivity of more than eight orders of magnitude is observed after annealing at 1000 °C for the samples irradiated by H_2^+ ions with only eight times different doses (Fig. 3). At the same time, the conductivity is practically absent along the surface and low enough between one contact tungsten needle on the chemically treated surface and another one on the contact pad (Fig. 4a). In the last case, clearly superlinear behavior is observed due the injection of the charge carriers in high electric fields (~10^6 V/cm) and their trapping on the defect states leading to space charge limited current (SCLC) [13].

3.2. Temperature dependent resistance measurements

Annealing temperature dependences of the conductivity for NG samples are presented in Fig. 5, where the slopes of the curves show the activation energy for changes in conduction. If the conduction is proportional to the carrier concentration according to Baskin's model [16], then we can compare this activation energy with the concentration of the defects responsible for the carrier generation. Simple neutral vacancy defects (or GR1 centers) have the same activation energy $E_a^{GRI} = 2.43$ eV as the concentration of the carriers [24]. It seems likely that vacancy migration is responsible for the annealing of charged defects at moderate temperatures in our samples. But this coincidence may be casual due to the deep level nature of defect centers in the diamond. In this case the conductivity cannot be proportional to the concentration. To study the nature of conductivity the temperature dependences of the buried layer sheet resistivity were investigated using wider temperature interval of annealing (500 ÷ 1300 °C) and measurements (4 ÷ 500 K).

The results of the RT measurements for the structures with cleaved and polished surfaces are presented in Fig. 5. There are differences in sheet resistance behavior of two sets of DC and NG samples, where for fluences lower than 4×10^{16} cm^{-2} the resistance increases for polished samples only. A decrease in resistance for cleaved DC samples correlated with starting of blistering visible by AFM measurements. For polished NG samples, the blistering was observed also in optical microscope for fluences higher then 6×10^{16} cm^{-2} and temperature 1300 °C (inset on Fig. 6b). Blistering for highest investigated fluence 1.3×10^{17} cm^{-2} was minimal after annealing at 1250 °C.

Changes in the sheet conductance $\sigma_s = 1/\rho_s$ in dependence on the temperature of measurements to the power of $-1/4$ are shown on the Fig. 6 for cleaved samples implanted with lowest and highest doses and isochronal annealing at 1100 °C during 1 h.

Straight lines represent a good approximation of the experimental dependences for the temperature of measurements in the

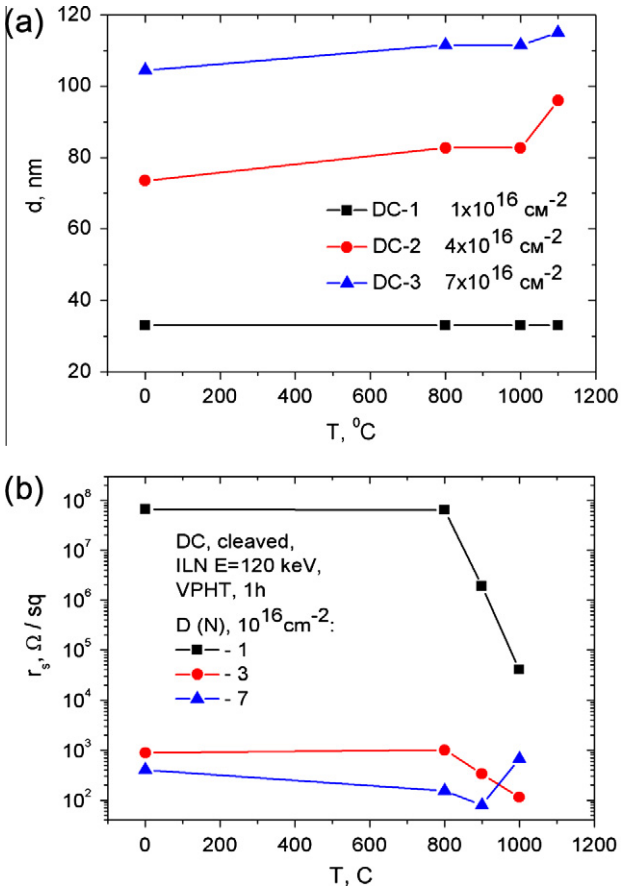

Fig. 2. (a) Plots of 0.5×2 mm^2 contact pads height measured by AFM on the cleaved surface of diamond plates formed by N^+ ion implantation after different temperatures of annealing; (b) the same but for the sheet resistivity of the pads.

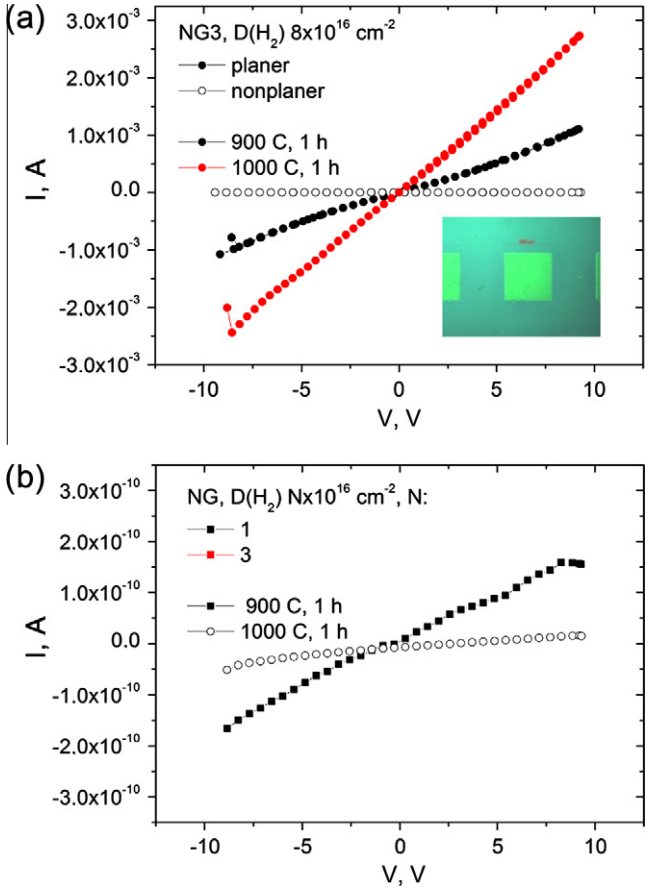

Fig. 3. (a), (b) I–V – characteristics measured between two neighbor pads (on inset) for samples annealed at 900 and 1000 °C during 1 h for highest and lowest doses respectively.

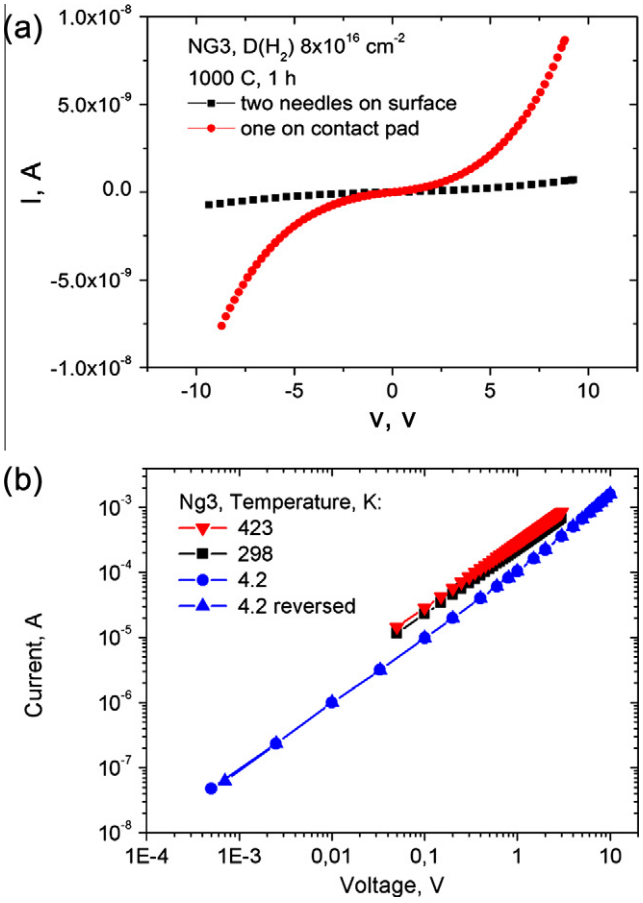

Fig. 4. (a) IV characteristics measured between square pad and W needle on the surface for sample NG3 implanted with H_2^+ fluence 8×10^{16} cm^{-2} and annealed at 1000 °C during 1 h; (b) the same but for the needles placed on the contact pads for three different temperatures.

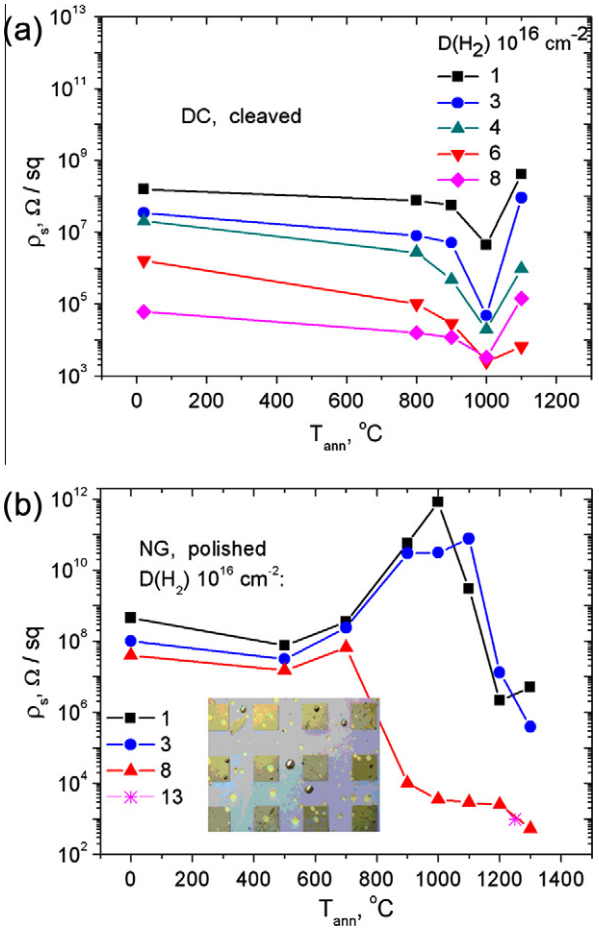

Fig. 5. (a) The sheet resistance of buried layer for cleaved samples with $0.5 \times 2 \times$ mm^2 contact pads for RT; (b) the same but for polished samples, where the blistering and exfoliation are shown on the inset for NG3 sample optical microphotography after 1300 °C 1 h annealing.

power of −¼. This dependence corresponds for theoretical predictions in the case of variable range hoping mechanism of the conductivity through well localized deep states in the forbidden band of wide gap semiconductors [15,25]:

$$\sigma_s(T) = \sigma^*_{s0} T^{1/2*} exp[-(T_0/T)^{1/4}] \quad (1)$$

where $T_0 = 512/(9\pi a^3 k_B N(E_F))$, a is a decay length of wave functions for localized states for jumps, $N(E_F)$ is the density of these states near Fermi level. Such behavior is seen clearly on the Fig. 6a) for the lowest fluence of hydrogen. Slow deviations are visible for the higher fluence due to beginning of formation of the inner surfaces inside the buried layer, followed by blistering. These surfaces provide a parallel way for the carrier flow along the implanted layer and should have another power law dependence for 2D transport equal to −1/3[14].

We estimated the dependence of the value $N(E_F)$ as $N(E_F) = 16/a^3 k_B T_0$ for different samples on the dose and annealing temperatures (Fig. 7), where T_0 values were obtained from slopes like on the Fig. 6, and $a = 1.2$ nm for sp2 bond [25]. The critical dose for irreversible increase in the density $N(E_F)$ coincides with the critical dose obtained for sheet resistivity from Fig. 5b. But accumulation of these states does not follow single exponential Arrhenius dependence (Fig. 7). It means that at least two different kinds of the defects (not only sp2 bonds) participate in charge transport. Nonmonotonic dependence of the conductivity on hydrogen content also corresponds to the model of phase transition in implanted diamond layer to another allotropic form of carbon. According to the literature, such a transition depends strongly on the "critical" dose of implanted ions, which is determined by the critical concentration of the vacancies $\sim 1 \times 10^{22}$ cm^{-3} [2]. The critical dose for nitrogen ions is only 5×10^{14} cm^{-2}, while it is much higher for light hydrogen molecules $\sim 1 \times 10^{16}$ cm^{-2}. There are evidences that for buried defects, the critical concentration is about 5–10 times higher [13]. These values satisfy the conditions needed for graphitization in the bulk of our samples for the case of highest hydrogen fluences and up to the surface in the case of nitrogen implantation. To determine the nature of other states we have investigated $\sigma_s(T)$ dependences for NG samples in wider temperature range $4 \div 500$ K with two different functional dependences (Fig. 8) one for VRH model and another one for quantum corrections to conductance, which are characteristic for disordered metallic systems [26]:

$$\sigma(T) = \sigma(0) + \Delta\sigma_{e-e}(T) = \sigma(0) + \beta \cdot T^{1/3}, \quad (2)$$

where $\Delta\sigma_{e-e}(T)$ is a quantum correction due to mutual electron interference in the diffusion channel. As it follows from the data (Fig. 8) these both dependencies can satisfactory be fitted by the straight line for sample NG3 annealed at the temperature 1000 °C. It means that the electronic system in this layer is very close to the metal–insulator transition (MIT).

The crossing of the straight lines on Fig. 8b with 0 give $\sigma(0)$ value, the sign of it determines on which side of MIT there is a system. The positive one coincides with metallic character, while

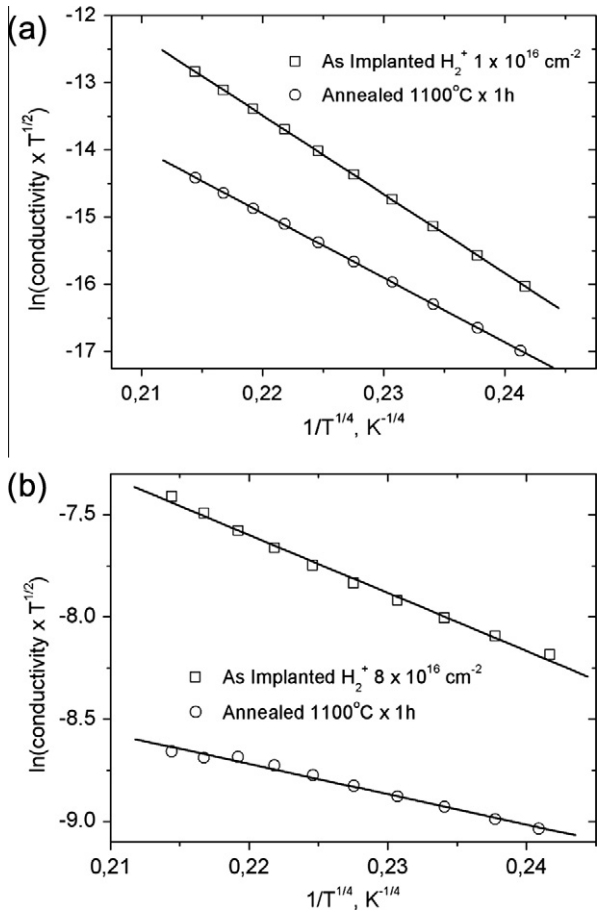

Fig. 6. (a) Temperature dependencies of the sheet conductivity for buried layers in DC samples implanted with hydrogen fluence 1×10^{16} cm^{-2} after 1100 °C, 1 h; (b) the same but for the fluence 8×10^{16} cm^{-2}.

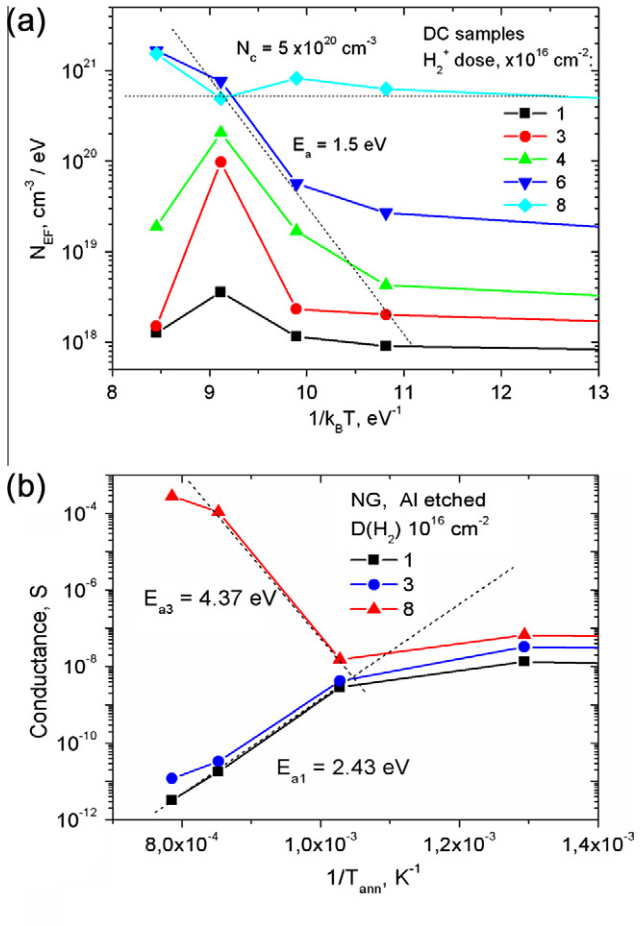

Fig. 7. (a) Localized deep state densities $N(E_F)$ for DC samples in dependence on the annealing temperature, where the absent of Arrhenius dependence is visible; (b) dependencies of the conductance on the reverse temperature of annealing for three samples implanted with different hydrogen doses.

the negative one means dielectric behavior. Integrating $N(E_F)$ states only near E_F in the band width $\sim kT = 0.026$ eV, gives the carrier concentration about the same as in Van-der-Pauw measurements $n = 5.2 \times 10^{20}$ cm^{-3} at RT. Essentially the density of states $N(E_F)$ at Fermi level is much higher for cryogenic temperature interval of the measurements (Table 1).

The $N(E_F)$ data from Table 1 seems too high in comparison with EPR data [9], especially for low temperature conductance, where the density of states $N(E_F)$ even higher than the density of atoms in diamond 1.76×10^{23} cm^{-3}.

Another important parameter can be determined from the plots like Fig. 8a. This quantity is the value of $\ln(\sigma_{0,Mott})$, when $T \to \infty$ i.e. at the cross of the plots with vertical axis at $x = 0$. Godet model for VRH mechanism with exponential density of states $N(E_F)$ in the form of $N(E) = (N_0/E_0)\exp((E-E_F)/E_0)$, where E_0 is a distance from Fermi level to percolation level, shows universal character for the disordered semiconductor systems including amorphous carbon [15].

If $E_o >> kT$ Band-Tail-Hopping (BTH) mechanism predicts, that the slope of the dependence $\ln S_0 = f(T_0)$ for semiconductor system is always positive and linear: $\ln S_0 = B(T_0)^{1/4} + C$, where $B > 0$.

Our data for this dependence presented on Fig. 9 do not show monotonic relation between these quantities. It means that in our electronic system there is also another mechanism for electronic transport.

3.3. AFM and Raman spectroscopy measurements

Structural and phase changes were investigated for the higher fluences implantation and followed by VPHT and HPHT treatments for NG- and B-series of the samples to prove the result of electrical measurements. According to AFM data glassy carbon (gl-C) layers do not show phase contrast, but have about 40% loss in their density relative to diamond. The results of Raman investigation for the B samples after implantation and annealing at 1200 °C are shown in Fig. 10. Formation of new phases in treated samples are proved by the appearance of, beside the narrow diamond optical phonon line at 1332 cm^{-1}, new wide peaks at 1327, 1360, and 1580 cm^{-1}, related to tensile stressed diamond, defects in sp2 aromatic rings (D-band), and vibration bending mode in perfect graphite rings (G-band), respectively [28]. Raman spectroscopy with AFM measurements for partially delaminated films present clear evidences of nanometer thick (30–50 nm) upper diamond (nd-C) layer and buried glassy like carbon (gl-C) layers formed for highest fluences. AFM and Raman spectra show highly homogenious flat gl-C layer with thickness 10 ÷ 300 nm and ratio for the areas of D- and G-lines varied from 10 to ~2 with increasing of the fluence for HPHT samples, while for VPHT this ratio was unchanged near ~1.2.

It is well known, that the full width at half maximum (w_G) of G-band and the ratio of two bands may serve as a measure of graphite phase quality or can be used to estimate dimensions of graphite flakes in nanocrystalline graphites.

According to the investigation of Larouche and Stansfield [28], the best criterion for this purpose is the ratio of band areas A_D/A_G. To obtain these values, the experimental Raman spectra were deconvoluted by Origin™ 8.0 software. The areas of D- and G-lines were determined as a product $I\,w$, where I is a peak height and w is

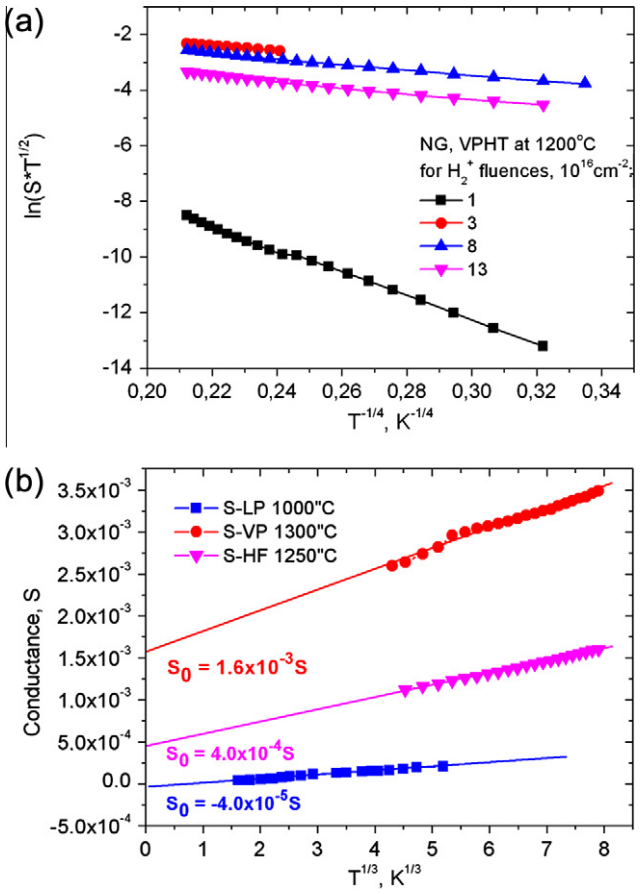

Fig. 8. (a) The same as on Fig. 6 but for NG samples; (b) the conductance dependencies on the temperature in power 1/3 for NG3 and NG9 samples with two highest hydrogen molecule fluences (8×10^{16} cm^{-2}, 1.3×10^{17} cm^{-2}) and different annealing temperatures.

a full width at half maximum (FWHM), obtained by the Lorentzian or Gaussian deconvolution technique. If this ratio is proportional to the graphite nanocrystal size L_a according to the relation $L_a = 4.4 (I_D w_D / I_G w_G)^{-1}$ [nm] from work [28], then it gives $L_a = 2$ nm in gl-C layer formed during HPHT inside the diamond substrate, while for VPHT treated samples they are essentially larger. The upper nd-C layer ($30 \div 50$ nm) is less uniform and has strong shift of the diamond line from 1332 to 1327 cm^{-1}. The same relation gives for graphite flake diameter only $L_a = 1$ nm. These flakes may provide tensile stresses in upper diamond film, which lead to an observed the Raman shift of the diamond line to the low energy of phonons.

Another important feature of HPHT treated samples is a wide band of lines between 1400 and 1500 cm^{-1}. These Raman lines are attributed mainly in the literature to C=C bonds in olephetic chains and do not appear or are very weak in the case of VPHT treatment. Flake dimensions for all heavily implanted samples are summarized in Table 2, together with the graphite band width

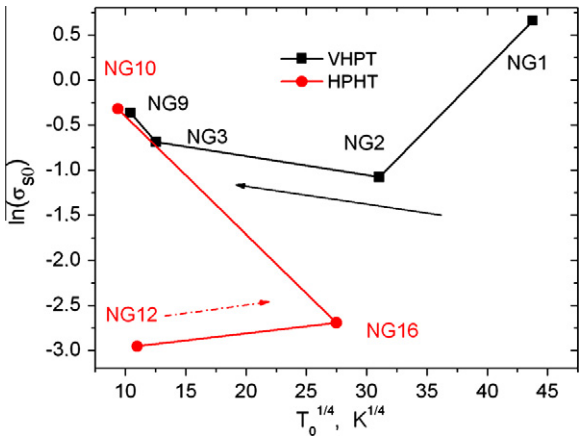

Fig. 9. Plots of relation between $\ln(\sigma_{s0})$ and $T_0^{1/4}$ for NG samples annealed at 1200 °C under vacuum (NG1–NG9, VPHT) or high pressure (NG12–NG10, HPHT).

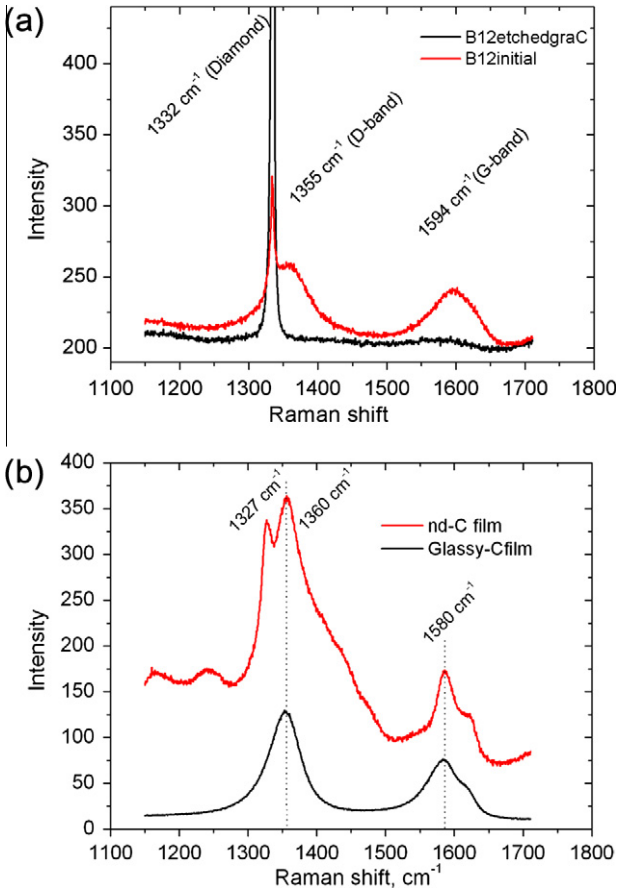

Fig. 10. Raman spectra for for B samples annealed at 1200 °C; (a) under vacuum (B12, VPHT); (b) under high pressure (B13, HPHT).

Table 1
Density of states $N(E_F)$ [cm^{-3} eV^{-1}] at Fermi level for $a = 1.2$ nm (sp^2 bonds) according to Eq. (1) after hydrogen implantation with the fluence Φ [cm^{-2}] and followed LPHT, VPHT and HPHT treatment at temperature T_{ann}.

Φ/T_{ann}	As impl.	600 °C	800 °C	1000 °C[a]	1200 °C	1200 HP	1300 °C
1×10^{16}	–	–	–	8×10^{18}	8×10^{18}	–	3.0×10^{19}
3×10^{16}	–	–	–	2.0×10^{22}	7×10^{19}	7.4×10^{21}	1.2×10^{20}
8×10^{16}	8×10^{17}	1×10^{18}	4×10^{21}	2.5×10^{23}	2.0×10^{22}	1.9×10^{20}	1.1×10^{22}
13×10^{16}	–	–	–	–	4.3×10^{21}	1.2×10^{22}	–

[a] The data were determined at cryogenic temperatures of $\sigma(T)$ measurements.

Table 2
Raman graphitization indices [28] and density of states $N(E_F)$ [cm^{-3} eV^{-1}] for NG- and B-series of samples for variable decay length a after hydrogen implantation with the fluence Φ [cm^{-2}] and followed VP or HP treatment at annealing temperature T_{ann}.

Φ/T_{ann}	L_a 1200 °C	Gauss/Lorentz	w_G/cm^{-1}	$N(E_F)$ 1200 °C	L_a 1200 HP	Gauss/Lorentz	w_G/cm^{-1}	$N(E_F)$ 1200 HP
8×10^{16}	0.3	L	39	1×10^{16}	1.2	L	65	1.0×10^{14}
13×10^{16}	3.4	G	67	2.0×10^{16}	2.9	L	48	1.5×10^{16}
-,B-dop.	5.5	G	60	–	2.3	L	50	–
-, -, gl-C	3.1	G	50	–	1.3	L	30	–

(w_G) and corrected values for density of states $N(E_F)$ for variable decay length a (determined in the next part of the article).

Upper diamond (nd-C) and buried glassy like carbon (gl-C) layers in heavily implanted samples were exfoliated by further treatments and also were investigated separately. No essential differences were observed in their properties after lift-off procedure.

4. Discussion

According to the revised VRH model of Achats et al. [27], $\sigma_{0,Mott} = S_0$ depends on the decay length a as:

$$S_0 = (1/32\pi)^{1/2}(aN(E_F)/k_B)^{1/2}e^2 v_{pn} \quad (3)$$

where e is an electron charge and v_{pn} is an optical phonon frequency $\sim 10^{12}$ s^{-1} for disordered medium.

Using the expression for T_0 [14] it is possible to obtain the value of hopping decay length a from the experimentally determined values S_0 and T_0 (Fig. 9):

$$a = 4/3 \cdot \pi^{-1}\ e^2\ v_{pn} k_B^{-1}\ S_0^{-1}\ T_0^{-1/2} \quad (4)$$

This expression does not contain an explicit form of $N(E_F)$ dependence and allows to estimate an optimum hopping jump length R_h from the experimentally determined a value. These data are presented on Fig. 11. Hopping decay length a ($1 \div 10$ nm) seems too low for VPHT samples implanted with low fluencies of hydrogen. A simple relation follows from the data on Fig. 11a:

$$a = -D \cdot (T_0)^{1/4} + E, \quad (5)$$

where $D > 0$ and crossing at $T_0 = 0$ determines a decay length a for MIT: $a_{MIT} = 140$ nm. This value is very close to a values determined for heavily implanted and VPHT treated samples and explains their "quasimetallic" behavior described by Eq. (2).

The optimum hopping length R_h determined according to Mott as $R_{h,Mott} = 3a/8(T_0/T)^{1/4}$ [15,27] gives $R_{h,Mott} \approx 100$ nm at room temperature for NG2–NG9 samples treated at VPHT conditions (Fig. 11b).

It means that the medium, which determines electron transport, is homogeneous in phase content and nearly independent on the hydrogen fluence. This may be true if the thickness of this buried layer increases with H_2^+ fluence. The increase in the thicknesses of gl-C layers was really observed by AFM measurements by the step height between lithographically determined initial and irradiated surfaces, which grow from initial 10 nm height for the fluence of 6×10^{16} cm^{-2} up to 300 nm for the fluence of 1.3×10^{17} cm^{-2} after annealing at 1200 °C.

Moreover, revised hopping decay length a allows to correct $N(E_F)$ values in Table 1 for VPHT and HPHT treated samples after annealing at 1200 °C. According to them, the maximum value of $N(E_F) = 8 \times 10^{18}$ cm^{-3} eV^{-1} is observed for lowest fluence of hydrogen molecule implantation, while with its increasing it drops to $N(E_F) = 2 \times 10^{16}$ cm^{-3} eV^{-1} and remains practically constant for all VPHT treated samples (Table 2).

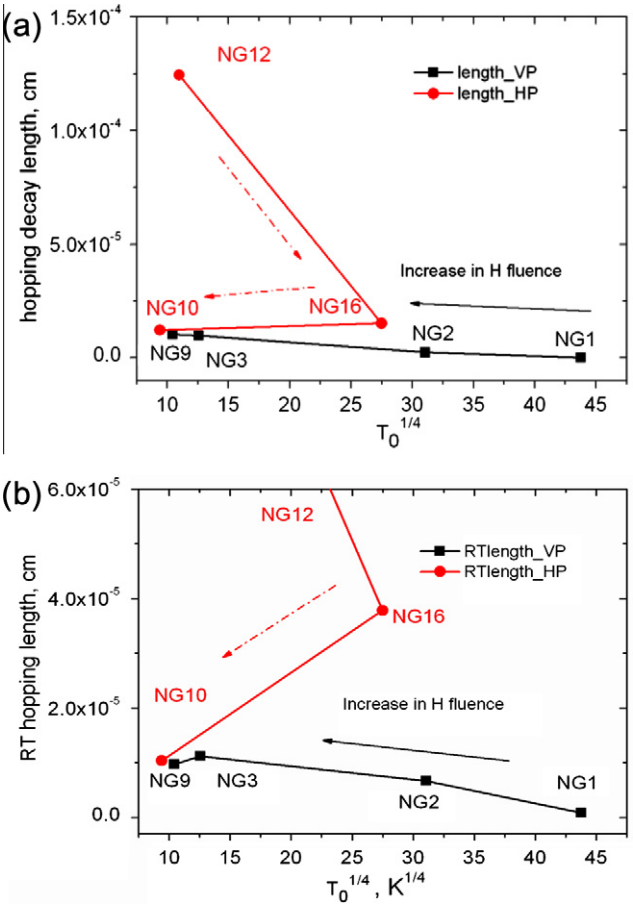

Fig. 11. (a) Hopping decay length a for localized state wave functions; (b) optimum hopping length R_h at room temperature for NG samples annealed at 1200 °C under vacuum (NG1–NG9, VPHT) or high pressure (NG12–NG10, HPHT).

A quite different picture was observed for HPHT samples where all quantities (S_0, T_0 and $N(E_F)$) do not correlate with hydrogen fluencies providing a decrease in hopping decay length with increasing fluence (Fig. 11a). One possible reason is the structural changes in HPHT samples that were confirmed by Raman spectroscopy, giving clear evidence of graphite phase clusterization. It was suggested previously, that such clusterization leads to the delocalization of charged carrier wave functions [29,30]. This idea coincides also with our results obtained by electric measurements, where decay lengths as high as 1 μm were observed after medium fluence and HPHT treatments despite of the lower conductivity and very low $N(E_F)$ in the buried layers. Further increase in the H fluence decreases G-band width w_G, but unexpectedly decreases the decay length a.

It is remarkable from the data of Table 2 that there are no correlations between averaged nanocrystalline graphite flake dimension L_a and density of states $N(E_F)$. It means that the average

dimensions of the flakes are not essential for transport properties of charge carriers in buried layers in heavily implanted samples. More essential quantity for electrical transport is a length of curved graphene planes L_e, which provide other mechanisms and determine their conductivity [30].

We studied by electron microscopy in TEM and HREM modes the structures of delaminated films and showed that the thick buried layers are amorphous with inclusions in the form of 1–3 nm length graphite flakes in VPHT treated samples. HPHT treated samples show a formation of thin intermediate epitaxial layer ($\sim$10 nm) with different from graphite and diamond lattice between upper diamond nd-C and buried amorphous gl-C layers. Variability in decay length a leads to a constant RT hopping range R_h in buried gl-C layers with varied thicknesses after VPHT treatment in the wide range of fluences, but for lower fluences this decay length coincides with the length of graphite flakes, observed by Raman spectroscopy and HREM.

The conductivity model should also take into account a transport way in few nanometer thick new phase layers formed in HP annealed samples between the surface nd-C and buried gl-C layers according to HREM data. Charge carrier transport in HPHT annealed samples after low fluences is described by very low density of states $N(E_F) < 1.0 \times 10^{14}$ cm^{-3} with weakly localized wave functions a due to a presence of the graphite flakes inside gl-C buried layers near the upper interface. But both the experimental data and the model could be improved further.

5. Conclusions

Electrical measurements and Raman spectroscopy show that buried conductive layers are formed after vacuum (VPHT) and few GPa pressure (HPHT) thermal treatments if the hydrogen fluences exceed the critical value $\Phi_C = 4 \times 10^{16}$ cm^{-2} for chosen energy 50 keV per hydrogen molecular ions. In that cases the conductive glassy carbon (gl-C) layers are formed and have the thickness from 10 to 300 nm with low sheet resistance $\rho_s = 1$ kΩ/sq for VPHT, and more than two order of magnitude higher $\rho_s = 3 \times 10^5$ Ω/sq for HPHT. Dominant conductivity mechanism is variable range hoping (VRH) on defect states for temperature range 4–525 K. For heavily implanted samples with highest conductivity it is changed showing quasimetallic behavior.

Two or three order of magnitude differences in the conductivity for VP and HP annealed samples are attributed to the higher dimensions of graphite nanocrystalline inclusions in buried glassy carbon (gl-C) layers in the case of vacuum annealing. This suggestion coincides with Raman spectra and determined optimum hopping length R_h in VRH model.

Conductivity model also should take into account a parallel transport path in few nanometer thick new phase layer formed in HPHT annealed samples between surface nd-C and buried gl-C films. Charge carrier transport in these samples is described after low hydrogen fluences by low density of states $N(E_F)$ with weakly localized wave function decay length a due to a presence of this layer. But both the experimental data and the model should be improved further for deeper understanding of the physics behind phase transition and conductivity in buried layers in diamond after hydrogen heavy implantation and HPHT thermal treatment, which will be presented in the next publications.

Acknowledgment

The authors would like to thank the colleagues from the Institute of Semiconductor Physics: Dr. V.A. Volodin for Raman spectroscopy; Dr. A.K. Gutakovskii for HREM investigation; Dr. V.G. Erkov for cryogenic electrical measurements; E.D. Zhanaev for chemical etching and sample preparation. Additional thanks goes to the project fellows from Institute of Geology and Mineralogy for HPHT treatments and fruitful discussions. Finally the authors express their gratitude to the Presidium of Siberian Branch of Russian Academy of Science for financial supporting the Integration Project No. 68/09-11.

References

[1] A.J. Neves, Maria Helena Nazaré. Properties, growth and applications of diamond. INSPEC. (EMIS Group-Science – 2001) p. 427.
[2] Johan F. Prins, Semicond. Sci. Technol. 18 (2003) S27.
[3] Johan F. Prins, J. Phys. D: Appl. Phys. 34 (2001) 2089.
[4] R.A. Khmelnitsky, V.A. Dravin, A.A. Gippius, J. Chem. Vapor Depos. 5 (1996) 121.
[5] A.A. Gippius, R.A. Khmelnitsky, V.A. Dravm, S.D. Tkachenko, Diamond Relat. Mater. 8 (1999) 1631.
[6] A.A. Gippius, R.A. Khmelnitsky, V.A. Dravin, A.V. Khomich, Physica B 308–310 (2001) 573.
[7] A.A. Gippius, R.A. Khmelnitsky, V.A. Dravin, A.V. Khomich, Diamond Relat. Mater. 12 (2003) 538.
[8] R.A. Khmelmtskiy, E.V. Zavedeev, A.V. Khomich, A.V. Gooskov, A.A. Gippms, Vacuum 78 (2005) 273.
[9] A.V. Khomich, N.A. Poklonskii, N.M. Lapchuk, R.A. Khmel'nitskii, V.A. Dravin, S. Munkhtsetseg, J. Appl. Spect. 74 (2007) 537.
[10] T.I. Galkina, A.Yu. Klokov, A.I. Sharkov, R.A. Khmelnitskii, A.A. Gippius, V.A. Dravin, V.G. Ral'chenko, A.V. Savel'ev, Physics of Solid State 49 (2007) 654.
[11] P. Olivero, G. Amato, F. Bellotti, et al., Diamond Relat. Mater. 18 (2009) 870.
[12] P. Olivero, G. Amato, F. Bellotti, S. Borini, A. Lo Giudice, F. Picollo, Eur. Phys. J. B 75 (2010) 127.
[13] H. Wang, P. Olivero, M. Bruna, et al., IOP Conf. Ser.: Mater. Sci. Eng. 16 (2010) 012004.
[14] N. Mott, Conduction in Non-Crystalline Materials, second ed., Oxford Science Publcations, New York, 1993. p. 150.
[15] C. Godet, Philos. Mag. B 81 (2001) 205.
[16] E. Baskin, A. Reznik, D. Saada, J. Adler, R. Kalish, Phys. Rev. B 64 (2001) 224110.
[17] C.F. Wang, R. Hanson, D.D. Awschalom, E.L. Hu, T. Feygelson, J. Yang, J.E. Butler, Appl. Phys. Lett. 91 (2007) 201112.
[18] J.R. Maze, P.L. Stanwix, J.S. Hodges, et al., Nature 455 (2008) 644.
[19] M. Liao, S. Hishita, E. Watanabe, S. Koizumi, Y. Koide, Adv. Mater. 22 (2010) 5393.
[20] B.A. Fairchild, P. Olivero, S. Rubanov, et al., Adv. Mater. 20 (2008) 4793.
[21] A. Stacey, V.S. Drumm, B.A. Fairchild, et al., Appl. Phys. Lett. 98 (2011) 181907.
[22] J.O. Orwa, C. Santori, K.M.C. Fu, et al., J. Appl. Phys. 109 (2011) 083530.
[23] Yu.N. Palyanov, Yu.M. Borzdov, A.F. Khokhryakov, I.N. Kupriyanov, A.G. Sokol, Crystal Growth & Design 10 (2010) 3169.
[24] L. Allers, A.T. Collins, J. Hiscock, Diamond Relat. Mater. 7 (1998) 228.
[25] A. Reznik, V. Richter, R. Kalish, Physical Review B 56 (1997) 7930.
[26] I. Shlimak, M. Kaveh, R. Ussyshkin, V. Ginodman, L. Resnick, Phys. Rev. Lett. 77 (1996) 1103.
[27] P. Achats, O.A. Williams, P. Bruno, D.M. Gruen, J.A. Garrido, M. Stutzmann, Phys. Rev. B 74 (2006) 155429.
[28] N. Larouche, B.L. Stansfield, Carbon 48 (2010) 620.
[29] J.D. Carey, S.J. Henley, Diamond Relat. Mater. 16 (2007) 1782.
[30] F. Alibart, M. Lejeune, O. Durand Drouhin, K. Zellama, M. Benlahsen, J. Appl. Phys. 108 (2010) 053504.